# Wobble dC·dA Pairing 5′ to the Cationic Guanine N7 8,9-Dihydro-8-(N7-guanyl)-9-hydroxyaflatoxin $B_1$ Adduct: Implications for Nontargeted $AFB_1$ Mutagenesis†

Indrajit Giri‡ and Michael P. Stone*

*Department of Chemistry, Center in Molecular Toxicology, and the Vanderbilt-Ingram Cancer Center, Vanderbilt University, Nashville, Tennessee 37235*

*Received December 3, 2002; Revised Manuscript Received March 25, 2003*

ABSTRACT: The structure of 5′-d(ACATC[AFB]GATCT)-3′·5′-d(AGATCAATGT)-3′, containing the $C^5$·$A^{16}$ mismatch at the base pair 5′ to the modified $^{AFB}G^6$, was determined by NMR. The characteristic 5′-intercalation of the $AFB_1$ moiety was maintained. The mismatched $C^5$·$A^{16}$ pair existed in the wobble conformation, with the $C^5$ imino nitrogen hydrogen bonded to the $A^{16}$ exocyclic amino group. The wobble pair existed as a mixture of protonated and nonprotonated species. The p$K_a$ for protonation at the $A^{16}$ imino nitrogen was similar to that of the $C^5$·$A^{16}$ wobble pair in the corresponding duplex not adducted with $AFB_1$. Overall, the presence of $AFB_1$ did not interfere with wobble pair formation at the mismatched site. Molecular dynamics calculations restrained by distances derived from NOE data and torsion angles derived from $^1H$ $^3J$ couplings were carried out for both the protonated and nonprotonated wobble pairs at $C^5$·$A^{16}$. Both sets of calculations predicted the $A^{16}$ amino group was within 3 Å of the $C^5$ imino nitrogen. The calculations suggested that protonation of the $C^5$·$A^{16}$ wobble pair should shift $C^5$ toward the major groove and shift $A^{16}$ toward the minor groove. The NMR data showed evidence for the presence of a minor conformation characterized by unusual NOEs between $T^4$ and $^{AFB}G^6$. $T^4$ is two nucleotides in the 5′-direction from the modified base. These NOEs suggested that in the minor conformation nucleotide $T^4$ was in closer proximity to $^{AFB}G^6$ than would be expected for duplex DNA. Modeling studies examined the possibility that $T^4$ transiently paired with the mismatched $A^{16}$, allowing it to come within NOE distance of $^{AFB}G^6$. This model structure was consistent with the unusual NOEs associated with the minor conformation. The structural studies are discussed in relationship to nontargeted C → T transitions observed 5′ to the modified $^{AFB}$G in site-specific mutagenesis experiments [Bailey, E. A., Iyer, R. S., Stone, M. P., Harris, T. M., and Essigmann, J. M. (1996) *Proc. Natl. Acad. Sci. U.S.A. 93,* 1535−1539].

Aflatoxin $B_1$ ($AFB_1$)[1] is a highly mutagenic metabolite isolated from *Aspergillus flavus* and *Aspergillus parasiticus*. It is of health concern because of its potential to contaminate human food stocks (*1*). $AFB_1$ is a mutagen in bacteria (*2*−*4*); it is carcinogenic in fish (*5*, *6*), and it is a hepatocarcinogen in rodents (*7*, *8*). It is linked to the etiology of human liver cancer (*1*), possibly via adduct-induced mutations in the p53 tumor suppressor gene (*9*−*15*) and *ras* protooncogenes (*7*, *8*), and probably exacerbated by coinfection by the hepatitis B virus (*14*, *16*−*18*). It seems likely that $AFB_1$ is an important contributor to human cancer.

In humans, metabolism of $AFB_1$ by cytochrome $P_{450}$ 3A4 (*19*) yields $AFB_1$-*exo*-8,9-epoxide (*20*, *21*). Despite its relatively short half-life measured at 1 s (*21*), this epoxide reacts efficiently with duplex DNA to yield the cationic N7 adduct of deoxyguanosine *trans*-8,9-dihydro-8-(N7-guanyl)-9-hydroxyaflatoxin $B_1$ (*22*) (Scheme 1). The regioselectivity of adduction at the N7 position of deoxyguanosine is attributed to the precovalent intercalation of the epoxide above the 5′ face of deoxyguanosine (*23*). This places the $AFB_1$-*exo*-8,9-epoxide in close proximity and in the proper orientation to the N7 position of guanine, facilitating nucleophilic attack at the C8 position of the epoxide (*24*).

When M13 bacteriophages site-specifically adducted with the *trans*-8,9-dihydro-8-(N7-guanyl)-9-hydroxyaflatoxin $B_1$ adduct were inserted into *Escherichia coli* and evaluated as to replication (*25*−*27*), they induced low levels of G·C →

† This work was supported by NIH Grant CA-55678 (M.P.S.). Funding for the NMR spectrometers was supplied by Vanderbilt University, by NIH Grant RR-05805, and the Vanderbilt Center in Molecular Toxicology, ES-00267. The Vanderbilt-Ingram Cancer Center is supported by NIH Grant CA-68485.

* To whom correspondence should be addressed. Tel: (615) 322-2589. Fax: (615) 322-7591. E-mail: stone@toxicology.mc.vanderbilt.edu.

‡ Current address: Transgenomic Inc., 10 Corporate Place South, Third Floor, Piscataway, NJ 08854. Tel: (732) 981-0500.

[1] Abbreviations: $AFB_1$, aflatoxin $B_1$; EDTA, ethylenediamine tetraacetic acid; HPLC, high-pressure liquid chromatography; RT, room temperature; NOE, nuclear Overhauser enhancement; NOESY, two-dimensional NOE spectroscopy; COSY, correlation spectroscopy; DQF-COSY, double quantum filtered correlation spectroscopy; ROESY, rotating-frame Overhauser enhancement spectroscopy; ppm, parts per million; TPPI, time proportional phase increment; 1D, one-dimensional; 2D, two-dimensional. A right superscript refers to numerical position in the sequence starting from the 5′-terminus of chain A and proceeding to the 3′-terminus of chain A, and then from the 5′-terminus of chain B to the 3′-terminus of chain B. C2, C5, C6, C8, C1′, C2′, C2″, etc., represent specific carbon nuclei. H2, H5, H6, H8, H1″, H2′, H2″, etc., represent protons attached to these carbons. PEM, potential energy minimization; MD, molecular dynamics.

10.1021/bi020688n CCC: $25.00 
Published on Web 05/17/2003

Scheme 1: Structure of the *trans*-8,9-Dihydro-8-(N7-guanyl)-9-hydroxyaflatoxin $B_1$ Adduct and the Numbering Scheme for the Adducted Duplex d(ACATC$^{AFB}$GATCT)•d(AGATCAATGT) Containing the Mismatched $C^5$•$A^{16}$ Pairing Interaction

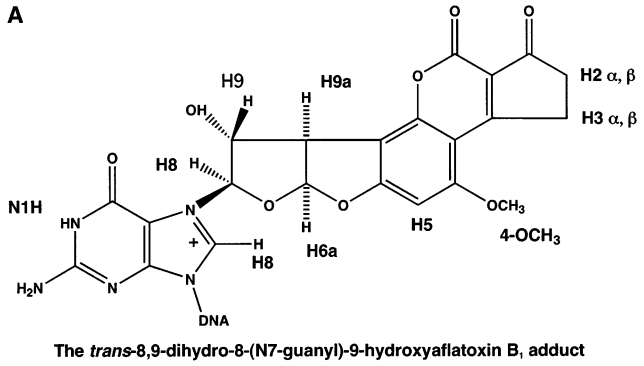


T•A base pair substitutions (*28*). These mutations were dependent upon expression of the damage-specific bypass polymerases MucAB and UmuDC. The G → T transversions were consistent with results of a forward mutation assay in which metabolically activated $AFB_1$ induced G → T transversions in the *E. coli lacI* gene (*3*). Of particular interest in the site-specific mutagenesis studies was the observation that 13% of the mutations induced by the $AFB_1$ adduct were nontargeted C → T transitions at the C•G base pair 5′ to the lesion site (*28*). This corroborated NMR studies indicating that the *trans*-8,9-dihydro-8-(N7-guanyl)-9-hydroxyaflatoxin $B_1$ adduct (*29*−*34*) and the corresponding deoxyguanosine N7 adduct of sterigmatocystin (*35*) intercalated above the 5′ face of the modified deoxyguanosine.

Because the site-specific mutagenesis experiments showed nontargeted C → T transitions at the 5′-neighboring base pair (*28*), it was of interest to examine the structure of a dC•dA mismatch located at the base pair 5′ to the $AFB_1$-modified deoxyguanosine. Previous studies of dC•dA mismatch pairing in DNA utilized both NMR (*36*−*38*) and X-ray crystallography (*39*). These suggested that the dC•dA mismatch existed in the wobble conformation, in which the exocyclic amino group of mispaired dA hydrogen bonded with the dC N3 imino nitrogen. Protonation of the mismatched adenine N1 position allowed formation of a second hydrogen bond, and stabilization of the dC•dA mispair. The stability of the dC•dA mismatch was dependent upon pH (Scheme 2) (*38*).

Here, the structure of 5′-d(ACATC$^{AFB}$GATCT)-3′•5′-d(AGATCAATGT)-3′, containing the $C^5$•$A^{16}$ mismatch at the base pair 5′ to the modified $^{AFB}G^6$ (Scheme 1), has been refined from NMR data and compared with the structure of the properly paired $C^5$•$G^{16}$ base pair 5′ to the $AFB_1$ adduct (*30*, *31*). The characteristic 5′-intercalation of the $AFB_1$ moiety is maintained. The $C^5$•$A^{16}$ mismatch exists in the wobble conformation, in which the imino nitrogen of $C^5$ hydrogen bonds with the exocyclic amino group of the mismatched $A^{16}$. The p$K_a$ of the $C^5$•$A^{16}$ wobble pair is comparable to that of the $C^5$•$A^{16}$ wobble pair in the corresponding duplex not adducted with $AFB_1$. The NMR

Scheme 2: Protonated and Nonprotonated Wobble Base Pairing for $C^5$•$A^{16}$ Mismatch: (A) Non-Protonated Wobble Pair and (B) Protonated Wobble Pair

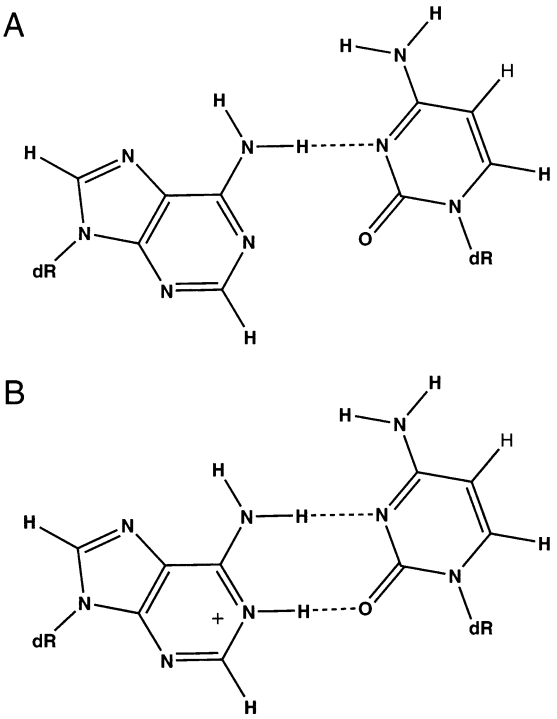


data show evidence of a minor conformation characterized by NOEs between $T^4$ and $^{AFB}G^6$. $T^4$ is two nucleotides in the 5′ direction from the modified base. Modeling studies have examined the possibility that in the minor conformation, $T^4$ is paired not with its complement $A^{17}$, but instead with mismatched $A^{16}$. This results in dislocation of nucleotide $C^5$, the nucleotide 5′ to the modified $^{AFB}G^6$, and complementary to the mismatched $A^{16}$. The model is consistent with the unexpected NOEs between $T^4$ and $^{AFB}G^6$. The presence of a minor strand dislocation structure provides a plausible rationale for nontargeted C → T mutations observed in site-specific mutagenesis experiments utilizing this $AFB_1$ adduct (*28*). These nontargeted mutations might be the consequence of dislocation mutagenesis (*40*, *41*) during error-prone lesion bypass. If transient dislocation of the damaged template strand occurs following correct incorporation of deoxycytosine opposite $^{AFB}G^6$, the error-prone replication apparatus might incorrectly use the 5′-next nearest neighbor nucleotide $T^4$ to template addition of an incoming dATP. Subsequent relaxation of the transient dislocation structure would position the stable $C^5$•$A^{16}$ wobble pair 5′ to the $AFB_1$-modified $^{AFB}G^6$•$C^{15}$ pair and enable primer extension beyond the damage site. If the resulting mismatch is not repaired, this could account for site-specific nontargeted C → T mutations 5′ to the cationic $AFB_1$ adduct observed in this sequence (*28*).

## MATERIALS AND METHODS

*Materials*. $AFB_1$ was purchased from Sigma-Aldrich Chemicals, Inc. (St Louis, MO). Unadducted oligodeoxynucleotides were purchased from Midland Certified Reagent Company (Midland, TX). The oligodeoxynucleotides were desalted using Sephadex G-25 (Pharmacia Biotech, Inc., Piscataway, NJ).

*Sample Preparation.* Dimethyldioxirane was prepared (*42*) and reacted at room temperature with $AFB_1$ to give $AFB_1$-

*exo*-8,9-epoxide (*20*). (Caution: Crystalline aflatoxins are hazardous due to their electrostatic nature and should be handled using appropriate containment procedures and respiratory mask to prevent inhalation. Aflatoxins can be destroyed by treatment with NaOCl. It should be assumed that aflatoxin epoxides are highly toxic and carcinogenic. Manipulations should be carried out in a well-ventilated hood with suitable containment procedures.) The oligodeoxynucleotide d(ACATC$^{AFB}$GATCT) was prepared by adding the epoxide dissolved in methylene chloride to an aqueous solution containing d(ACATCGATCT) dissolved in 2 mM sodium phosphate buffer (pH 7.5) at 5 °C in dark room, to form a two-phase mixture. Five equal aliquots of epoxide solution were added sequentially. The modified oligodeoxynucleotide was purified by HPLC using a C18 column (Hamilton, Inc., Reno, NV), equilibrated at room temperature and eluted with a 45 min gradient from 1% to 30% v/v acetonitrile in a 2 mM sodium phosphate buffer (pH 7.2), with a flow rate of 1.5 mL/min. The adducted oligodeoxynucleotide was desalted with Sepahadex G25 equilibrated with 0.1 mM phosphate buffer (pH 7.2). The adducted duplex d(ACATC$^{AFB}$GATCT)·d(AGATCAATGT) was prepared by titration of the complementary strand. The progress of the titration was monitored by NMR spectroscopy. Duplex formation was followed by monitoring the intensity of the aflatoxin H6a singlet at 6.63 ppm upon addition of the complementary strand. The integrity of the samples was examined periodically by HPLC because cationic guanine N7 adducts exhibit slow degradation due to spontaneous depurination.

*UV Melting.* Experiments were carried out on a Cary 4E spectrophotometer (Varian Associates, Palo Alto, CA). The buffer was 200 mM sodium phosphate, 0.05 mM $Na_2EDTA$, and 1 M NaCl at pH 7.0. The buffer solution was degassed prior to the experiment. The concentrations were adjusted to $4.8 \times 10^{-6}$ M in a 1 cm cuvette. The temperature was increased at a rate of 0.5 °C/min from 5 to 85 °C. Absorbance was measured at 260 nm. The melting temperatures of the native and modified oligodeoxynucleotides were calculated by determining the midpoints of the melting curves from the first-order derivatives.

*NMR Spectroscopy.* $^1$H NMR spectra were recorded at 500.13, 600.13, and 800.13 MHz. For observation of nonexchangeable protons, samples were dissolved in 0.5 mL of 0.01 M sodium phosphate buffer containing 0.1 M NaCl and 0.05 mM $Na_2EDTA$ at pD 7.2, and 6.7. Samples were dissolved in 99.96% $D_2O$. For observation of exchangeable protons, samples were dissolved in 9:1 $H_2O$:$D_2O$. Most experiments were performed at 5 °C. Spectra of exchangeable protons were obtained at both 0 and 5 °C. The temperature was controlled to ±0.5 °C. Phase-sensitive NOESY spectra with 250 ms mixing time were used for assignment of nonexchangeable protons. The watergate pulse sequence suppressed the water signal (*43*). The phase-sensitive NOESY spectra used in the nonexchangeable proton resonance assignments were recorded at 5 °C using TPPI quadrature detection. To derive distance restraints from NOESY data, three spectra were recorded consecutively at mixing times of 130, 180, and 250 ms, respectively. Typical acquisition parameters were as follows: 512 real data points in the d1 dimension with 32 acquisitions per FID, 2K real data points in the d2 dimension, relaxation delay of 2 s, and a sweep width in both dimensions of 8 kHz. Additional distance restraints were determined from NOESY spectra measured in $H_2O$ buffer and from NOESY spectra measured in $D_2O$ buffer using 3 s delay. Phase-sensitive DQF-COSY data were used to calculate the sugar pucker angles (*44*). NMR data were processed using FELIX (v. 2000, Accelrys, Inc., San Diego, CA) on Silicon Graphics (Mountain View, CA) Octane workstations. The data in the t1 dimension were zero-filled to give a matrix of 2K × 1K real points. A skewed sinebell-square apodization function with a 90° phase shift was used in both dimensions. Chemical shifts were referenced internally to the $H_2O$ peak.

*Distance Restraints.* Footprint boxes selected manually with FELIX fit well-resolved peaks at a contour level that showed the weak NOEs but not spectral noise. NOE-derived distances from cross-peak volumes measured at mixing times of 130, 180, and 250 ms were calculated using MARDIGRAS v3.2 (*45*, *46*). The volume error was one-half the volume of the smallest peak. Isotropic correlation times of 2, 3, and 4 ns were used. The RANDMARDI algorithm carried out 50 iterations for each set of data, randomizing peak volumes within limits specified by the input noise level (*46*). The standard deviation in a particular distance served as the error bound for the distance. Distance restraints were divided into classes weighted according to the error assessed in their measurement. Class 1, class 2, and class 3 distances were calculated from completely resolved, slightly overlapped, or medially overlapped cross-peaks, respectively, that were at least 0.5 ppm away from the water resonance or the diagonal line of the spectrum. Class 4 distances were calculated from all other cross-peaks. Empirical restraints preserved Watson−Crick hydrogen bonding except for the $C^5$·$A^{16}$ mismatch pair and prevented propeller twisting between base-pairs (*47*). NOEs that did not have a distance calculated by MARDIGRAS were assessed as strong, medium, or weak. These were assigned as 1.8−2.8, 1.8−3.8, or 1.8−5.0 Å, respectively. Negative restraints prevented protons for which no NOE was observed from moving closer than 5 Å.

*Dihedral Angle Restraints.* The deoxyribose DQF-COSY data were used to calculate the sugar pseudorotation, with the exception of $^{AFB}G^6$. Pseudorotation was determined graphically using sums of $^3$J $^1$H coupling constants from DQF-COSY data (*44*). These were fit to curves relating coupling constant to the pseudorotation angle (*P*), sugar pucker amplitude (Φ), and the percentage S-type conformation. The pseudorotation angle and amplitude ranges were converted to the dihedral angles $n_0$ to $n_4$. For d($A^1C^2A^3T^4$)·d($A^{17}T^{18}G^{19}T^{20}$) and d($A^7T^8C^9T^{10}$)·d($A^{11}G^{12}A^{13}T^{14}$), backbone torsion angles were empirically restricted to ranges, which would sample both A- and B-DNA. Force constants for the d($C^{5AFB}G^6$)·d($C^{15}A^{16}$) backbone torsion angles were one-half the magnitude of those used elsewhere in the molecule.

*Starting Structures.* A-DNA and B-DNA (*48*) structures containing the $C^5$·$A^{16}$ mismatch were built using INSIGHTII (Accelrys, Inc., San Diego, CA); these were named "IniA" and "IniB", respectively. In one set of structures, $A^{16}$ was protonated at the N1 position. In both instances, $AFB_1$ was intercalated above the 5′-face of $G^6$ (*29*). A bond between $AFB_1$ C8 and $G^6$ N7 was created. The adducted $^{AFB}G^6$ N7 was assigned $sp^2$ hybridization. Electrostatic potentials for

$^{AFB}G^6$ and N1-protonated $A^{16}$ were obtained from Hartree−Fock calculations using GAUSSIAN 98 (*49*) and basis set 6-31G* (*50*, *51*). The RESP module of AMBER 6.0 was used to derive the charges (*52*) from electrostatic potentials. The partial charges and AMBER atom type assignments for protonated $A^{16}$ and for $^{AFB}G^6$ are shown in Figures S1 and S2 in the Supporting Information.

*Potential Energy Minimization.* Conjugate gradient PEM calculations using X-PLOR (*53*) and the CHARMM force field (*54*) relaxed the starting structures described above. PEM calculations used to model the proposed minor conformation containing a transient $T^4$•$A^{16}$ base pair were restrained by two Watson−Crick hydrogen bonds assigned to $T^4$•$A^{16}$, using an error bound of ±0.5 Å. These were performed using the conjugate gradients routine in AMBER 6.0.

*Restrained Molecular Dynamics.* Calculations in vacuo without explicit counterions utilized X-PLOR (*53*) and the CHARMM (*54*) force field. The electrostatic term used the Coulomb function based on a reduced charge set of partial charges and a distance dependent dielectric constant of 4.0. The van der Waals term was approximated using the Lennard−Jones potential energy function. The cutoff radius for nonbonding interactions was 11 Å. The nonbonded pair list was updated if any atom moved more than 0.5 Å. The restraint energy function contained terms describing distance and dihedral restraints, both in the form of square well potentials (*55*). Bond lengths involving hydrogens were fixed with the SHAKE algorithm (*56*).

Calculations were initiated by coupling to a heating bath with a target temperature of 1000 K. Force constants of 10 kcal mol$^{-1}$ Å$^{-2}$ for empirical hydrogen bonding, 20 kcal mol$^{-1}$ Å$^{-2}$ for torsion angle restraints, and 50, 45, 40, 35, and 30 kcal mol$^{-1}$ Å$^{-2}$, for the five classes of NOE restraints, were used. The target temperature was reached in 5 ps and was maintained for 15 ps. The molecules were cooled to 300 K over 5 ps and maintained at that temperature for 25 ps of equilibrium dynamics. The force constants for the five classes of NOE restraints were scaled up for 3−5 ps during the heating period to 150, 130, 100, 100, and 100 kcal mol$^{-1}$ Å$^{-2}$, in the order of the confidence factors. These weights were maintained during the reminder of the heating period and for the first 5 ps of the equilibrium dynamics period. They were then scaled down to 50, 45, 40, 35, and 30 kcal/mol$^{-1}$ Å$^{-2}$ in the order of the confidence factors. The torsion angle and base pair distance force constants were scaled up to 100 kcal mol$^{-1}$ Å$^{-2}$ during the same period as for the NOE restraints. They were scaled back to 20 and 10 kcal mol$^{-1}$ Å$^{-2}$, also at the same time as the NOE restraints. The structure coordinate sets were archived every 0.1 ps, over the last 15 ps. These average rMD structures were subjected to 1100 iterations of conjugate gradient energy minimization. Convergence was monitored by pairwise calculations of rmsd for emergent structures.

The structures emergent from the X-PLOR calculations were solvated, and explicit counterions were added. The bond angle and improper torsion parameters were assigned by analogy to chemically similar types in the AMBER database Parm94.dat parameter set. Using the Leap module in AMBER 6.0, 17 $Na^+$ ions were added to neutralize the system containing the nonprotonated $C^5$•$A^{16}$ base pair; 16 $Na^+$ ions were added to neutralize the system containing the protonated $C^5$•$A^{16}$ base pair. The systems were solvated with a rectangular box of TIP3P waters (*57*) extending ∼10 Å from the DNA atoms in three dimensions. The solvated systems were equilibrated with the DNA structure fixed. Solvent equilibration involved four stages that totaled 140 ps of MD calculations in 1 fs steps. In the 30 ps first stage, the system was heated from 0 to 300 K, at constant volume, and with a 1 ps coupling constant to the temperature bath. In the 20 ps second stage, MD was continued at constant pressure to obtain the correct density at 300 K. In the 40 ps third stage, the coupling constant to the temperature bath was relaxed to 2.0 ps, and MD was continued at 300 K at constant pressure. During the first three stages of relaxation, a harmonic restraint of 5.0 kcal mol$^{-1}$ was used on the restrained atoms. In the 50 ps fourth stage, the MD was continued at constant volume and the DNA structure was allowed to relax. A harmonic force constant of 0.5 kcal mol$^{-1}$ was applied to the restrained atoms.

Subsequent rMD calculations of the solvated systems were performed, using the SANDER module of AMBER 6.0 (*58*) and the Cornell et al. force field (*59*), including the Parm94.dat parameter set. These were performed without artificial constraints for 200 ps. The systems were coupled to a 300 K temperature bath using a coupling constant of 1.4 ps. The Particle Mesh Ewald method (*60*, *61*) was employed to approximate Coulombic interactions. The SHAKE algorithm constrained bonds involving protons (tolerance = 0.0005 Å), and a 1 fs time-step was used throughout the simulation. The MD calculations ran for 1.0 ns, and coordinates were captured after every 200 steps to evaluate the dynamics.

*CORMA Calculations and Helical Analysis.* Calculation of NOE intensities from the structures emergent from rMD calculations utilized CORMA (*62*). Input volumes (intensities) were normalized from the intensities of protons with fixed internuclear distances (i.e., cytosine H5−H6 distance). Random noise was added to all intensities to simulate spectral noise. An isotropic correlation time ($\tau_c$) of 3 ns was used. The rotation of thymidine $CH_3$ groups was modeled using an 18-jump site model (*63*). A sixth root residual ($R_x^{1/6}$) factor was calculated for each structure (*64*). Helicoidal analysis was performed using the program 3DNA (http://rutchem.rutgers.edu/∼xiangjun/3DNA/) (*65*).

## RESULTS

*NMR Spectroscopy*. *A. pH Dependence*. NMR spectra of d(ACATC$^{AFB}$GATCT)•d(AGATCAATGT) were anticipated to show pH dependence because protonation of the $A^{16}$ N1 imino nitrogen would enable protonated $C^5$•$A^{16}$ wobble pairing. Spectra obtained from the unmodified oligodeoxynucleotide d(ACATCGATCT)•d(AGATCAATGT) at pH 4.8 and pH 7.8 showed the anticipated pH dependence, consistent with formation of a protonated wobble pair at the lower pH (*38*). Consequently, spectra of d(ACATC$^{AFB}$GATCT)•d(AGATCAATGT) were examined at pH 6.7, 7.2, and 7.8. Over this range of pH, $^1$H NMR spectra were characterized by line broadening of the mismatched $A^{16}$ aromatic H2 and H8 resonances, as well as for the mismatched $C^5$ aromatic H5 and H6 resonances. This was attributed, in part, to exchange broadening arising from protonated and nonpro-

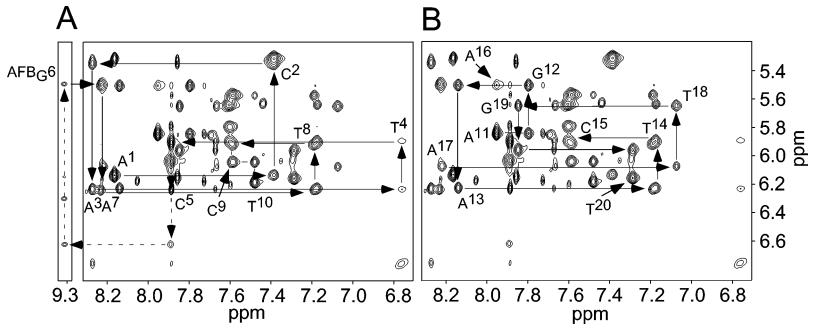


FIGURE 1: Expanded plots from the aromatic−anomeric region of the 600.23 MHz NOESY spectrum at 5 °C using a 250 ms mixing time, showing sequential NOE connectivities for (A) the modified strand and (B) the complementary strand. The resonances from $^{AFB}G^6$ were obtained in $H_2O$ buffer.

tonated populations of mismatched base pair $C^5$·$A^{16}$. It was not possible to examine a wider range of pH range because the cationic $AFB_1$ adduct was sensitive to depurination at acidic pH and to conversion to the corresponding formamidopyrmimidine (FAPY) derivative at basic pH. The $T_m$ of d(ACAT$\underline{C}^{AFB}$GATCT)·d(AGATC$\underline{A}$ATGT) was compared with that of d(ACAT$\underline{C}$GATCT)·d(AGATC$\underline{A}$ATGT). UV melting profiles demonstrated that the presence of $^{AFB}G^6$ resulted in a higher $T_m$ for this mismatched duplex at pH 7.2. In comparison to the unmodified mismatched duplex that exhibited a $T_m$ of 27 °C, the $AFB_1$-modified mismatched duplex showed an increased $T_m$ of 35 °C.

*B. DNA Proton Resonance Assignments*. The NOESY connectivity of the nonexchangeable protons (*66*) was affected both by the presence of the $C^5$·$A^{16}$ mismatch and the presence of the cationic $AFB_1$ lesion at base pair $^{AFB}G^6$·$C^{15}$ (Figure 1). In addition to being broad, the $T^4$ H6 resonance was observed at $\delta$ 6.8 ppm. This was approximately 0.5 ppm more upfield than its position in the corresponding $AFB_1$-modified oligodeoxynucleotide having correct base pairing at position $C^5$·$G^{16}$. In addition, the $C^5$ H5 and H6 resonances were shifted approximately 0.5 ppm downfield as compared to the corresponding adducted oligodeoxynucleotide having correct base pairing at $C^5$·$G^{16}$. The NOESY connectivity through the adducted strand was disrupted by the presence of the aflatoxin lesion. No connectivity was observed between $C^5$ H1′ → $^{AFB}G^6$ H8, observed at 9.33 ppm. The $^{AFB}G^6$ H8 proton exhibited NOEs to aflatoxin H6a as well as an intranucleotide NOE to $^{AFB}G^6$ H1′. The latter showed the expected NOE to $A^7$ H8 (Figure 1). Likewise, $C^5$ H6 exhibited a weak NOE to aflatoxin H6a, allowing sequential connectivity to be traced from $C^5$ to $A^7$ in the modified strand.

In the complementary strand, the presence of the mismatched $A^{16}$ strongly perturbed sequential NOE connectivities. The NOE between $C^{15}$ H1′ → $A^{16}$ H8 was weak. It was only observable at the longest mixing time. Its intensity increased at pH 7.8. Likewise, the $A^{16}$ H8 → $A^{16}$ H1′ cross-peak was weak, as was the $A^{16}$ H1′ → A17 H8 NOE. The $A^{17}$ H8 → $A^{17}$ H1′ NOE was of reasonable intensity but was broadened. The adenine H2 protons were assigned from NOEs with their own H1′ protons and the NOEs to the H1′ protons of the 3′-neighboring nucleotide. They showed NOE cross-peaks to the thymine N3H imino protons associated with their Watson−Crick pairing partners. The assignments of the DNA proton resonances are tabulated in Table S1, in the Supporting Information. Assignments for the deoxyribose

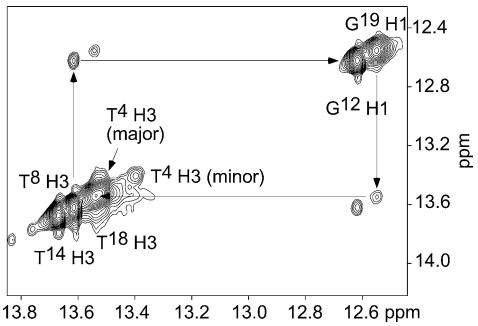


FIGURE 2: An expanded plot of the far downfield region of the 600.23 MHz NOESY spectrum in 90% $H_2O$: 10% $D_2O$ showing sequential NOE connectivities for the imino protons of base pairs $C^2$·$G^{19}$ → $T^4$·$A^{17}$ and $A^7$·$T^{14}$ → $C^9$·$G^{12}$. The labels represent the imino proton of the designated base.

protons were made primarily from DQF-COSY spectra. With the exception of the H5′ and H5″ resonances, unique assignments were made for all deoxyribose protons.

Two sharp resonances arising from imino protons were observed at $\delta$ 13.6 and $\delta$ 13.7 ppm, which were assigned to $T^8$ N3H and $T^{14}$ N3H, respectively (Figure 2). Two imino proton resonances overlapped at $\delta$ 13.5 ppm. These were assigned as $T^4$ N3H and $T^{18}$ N3H. The line broadening was attributed to $T^4$ N3H, suggesting enhanced exchange with water at base pair $T^4$·$A^{17}$. This observation was consistent with the broadening for nonexchangeable protons of base pair $T^4$·$A^{17}$ seen in Figure 1. This was the base pair 5′ to the $C^5$·$A^{16}$ mispair and the second base pair in the 5′-direction relative to $^{AFB}G^6$. In the 3′ direction, at the $AFB_1$ adduct site, $^{AFB}G^6$ N1H broadened to the extent it was not observable. The terminal $T^{10}$ and $T^{20}$ imino proton resonances were observed at $\delta$ 13.1 ppm. These resonances were broadened, suggesting rapid exchange with water. The hydrogen bonded and non-hydrogen-bonded amino protons for nucleotides $C^2$, $C^9$, and $C^{15}$ were observed as expected. For the mismatched $C^5$, only one amino resonance was observed, at $\delta$ 6.9 ppm. This was confirmed by an NOE to $C^5$ H5. The hydrogen bonded and non-hydrogen-bonded amino protons for nucleotides $A^3$, $A^7$, $A^{13}$, and $A^{17}$ were observed as expected. The hydrogen-bonded amino proton from mispaired $A^{16}$ was identified from an NOE to the $C^5$ amino protons. It also showed an NOE to the hydrogen bonded amino proton $A^{17}$ $N^6H_a$. These assignments are listed in Table S2 of the Supporting Information.

*C. Aflatoxin Proton Resonance Assignments*. A single set of resonances was observed for the $AFB_1$ protons (Figure 3). The connectivities between the furanose protons of

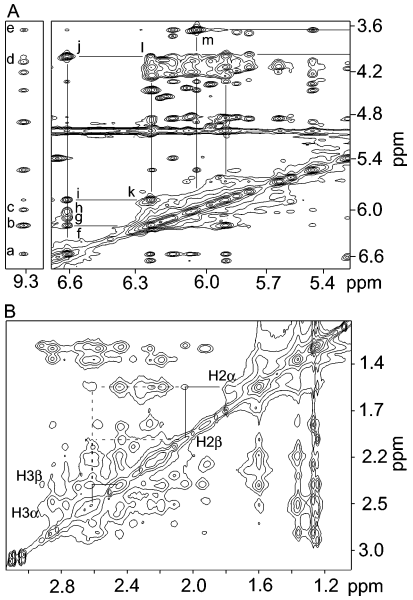


FIGURE 3: Expanded plot showing assignments for the $AFB_1$ moiety and cross-peaks between $AFB_1$ protons and the imidazole proton $^{AFB}G^6$ H8. (A) Downfield region of the $^1H$ spectrum. Cross-peaks a, $AFB_1$ H6a → $^{AFB}G^6$ H8; b, $AFB_1$ H8 → $^{AFB}G^6$ H8, c, $C^5$ H1′ → $^{AFB}G^6$ H8; d, $AFB_1$ H9a → $^{AFB}G^6$ H8; e, $AFB_1$ 4-$OCH_3$ → $^{AFB}G^6$ H8; f, $AFB_1$ H6a → $AFB_1$ H8, g, $AFB_1$ H6a → $C^5$ H5; h, $AFB_1$ H6a → $C^5$ H1′; i, $AFB_1$ H6a → $AFB_1$ H9; j, $AFB_1$ H6a → $AFB_1$ H9a; k, $AFB_1$ H8 → $AFB_1$ H9; l, $AFB_1$ H8 → $AFB_1$ H9a; m, $AFB_1$ H5 → $AFB_1$ 4-$OCH_3$. (B) Upfield region of the $^1H$ spectrum showing assignments of the cyclopentenone ring H2α, H2$\beta$, H3α, and H3$\beta$ protons.

aflatoxin located the $AFB_1$ H6a, H8, H9, and H9a resonances at $\delta$ 6.6, 6.3, 5.9, and 3.9 ppm, respectively, whereas the NOE between $AFB_1$ 4-$OCH_3$ and $AFB_1$ H5 located these resonances at $\delta$ 6.05 and 3.46 ppm. The methylene protons on the cyclopentenone ring were partially superimposed with the deoxyribose H2′ and H2″ protons as well as the thymine $CH_3$ protons. Stronger cross-peaks were observed between the diastereotopic geminal protons H2α and H2$\beta$, and H3α and H3$\beta$; weaker NOEs were observed between the vicinally coupled H2α, H2$\beta$, and H3α H3$\beta$ protons at each position.[2] The assignments of the $AFB_1$ $^1H$ resonances are listed in Table S3 of the Supporting Information.

*D. NOEs Between AFB₁ and the DNA.* A total of 32 NOEs were observed between $AFB^1$ protons and DNA protons; 10 of these were cross-strand NOEs involving mismatched $A^{16}$ (Table 1). Overall, the distribution of these NOEs was consistent with 5′-intercalation of the $AFB_1$ moiety at $^{AFB}G^6$. $AFB_1$ H6a and H9a, the protons located at the juncture of the fused furan rings, showed major groove NOEs in the 5′ direction, to $C^5$ of the mismatched $C^5$·$A^{16}$ base pair. Previous studies of the cationic $AFB_1$ adduct (*31*, *33*, *34*) showed strong cross-peaks between $^{AFB}$G H6a and H9a, and $C^5$ H6. In the present study, $AFB_1$ H6a showed a weaker cross-peak to $C^5$ H6, and $AFB_1$ H9a showed a weak NOE to $C^5$ H6 and no NOE to $C^5$ H5 at the mismatch site. $AFB_1$ H6a also showed NOEs to deoxyribose protons $C^5$ H1′, $C^5$ H2′, $C^5$ H2″, and $C^5$ H4′. The NOE to $C^5$ H4′ was possibly secondary, a consequence of spin diffusion in the deoxyribose ring. Both $AFB_1$ H6a and H9a showed NOEs to $^{AFB}G^6$ H8. Additional $AFB_1$−DNA cross-peaks were obtained from the $AFB_1$ 4-$OCH_3$ and $AFB_1$ H5 protons, located on the coumarin ring. The $AFB_1$ 4-$OCH_3$ protons showed NOEs to $C^5$ H6 and to $C^5$ H1′ and $C^5$ H2″. They also showed an NOE to $^{AFB}G^6$ H8. A cross-strand NOE was observed between $AFB_1$ 4-$OCH_3$ and $A^{16}$ H1′. $AFB_1$ H5 showed NOEs to deoxyribose protons $C^5$ H1′, $C^5$ H2′, and $C^5$ H4′. It also showed NOEs to $^{AFB}G^6$ H8, $^{AFB}G^6$ H1′, and $^{AFB}G^6$ H3′. $AFB_1$ H8 showed NOEs to $^{AFB}G^6$ H8 and $^{AFB}G^6$ H1′. $AFB_1$ H9 showed an NOE to $^{AFB}G^6$ H8. The remainder of the cross-strand NOEs with mismatched $A^{16}$ involved the cyclopentenone protons of $AFB_1$. NOEs were observed between $AFB_1$ H2α and $A^{16}$ H2, $A^{16}$ H8, $A^{16}$ H1′, $A^{16}$ H4′, $A^{16}$ H5′, and $A^{16}$ H5″ and between $AFB_1$ H2$\beta$ and $A^{16}$ H2. $AFB_1$ H3α showed NOEs to $A^{16}$ H2 and $A^{16}$ H4′. In all cases, the NOEs between the cyclopentenone protons of $AFB_1$ and $A^{16}$ H2 at the mismatch site were weak. These NOEs established the

Table 1: NOEs Observed between $AFB_1$ Protons and DNA Protons that Were Utilized as Restraints in the RMD Calculations

| $AFB_1$ proton | DNA protons |
|---|---|
| H2α | $A^{16}$ H2, $A^{16}$ H8, $A^{16}$ H1′, $A^{16}$ H4′, $A^{16}$ H5′, $A^{16}$ H5″ |
| H2$\beta$ | $A^{16}$ H2 |
| H3α | $A^{16}$ H2, $A^{16}$ H4′ |
| 4-$OCH_3$ | $C^5$ H6, $C^5$ H1′, $C^5$ H2″, $^{AFB}G^6$ H8, $A^{16}$ H1′ |
| H5 | $C^5$ H1′, $C^5$ H2′, $C^5$ H4′, $^{AFB}G^6$ H8, $^{AFB}G^6$ H1′, $^{AFB}G^6$ H3′ |
| H6a | $C^5$ H5, $C^5$ H6, $C^5$ H1′, $C^5$ H2″, $C^5$ H4′, $^{AFB}G^6$ H8 |
| H8 | $^{AFB}G^6$ H8, $^{AFB}G^6$ H1′ |
| H9 | $^{AFB}G^6$ H8 |
| H9a | $C^5$ H5, $C^5$ H6, $^{AFB}G^6$ H8 |

Table 2: Structural Refinement Statistics for the Nonprotonated RMD-Generated Structures of the *trans*-8,9-Dihydro-8-(N7-guanyl)-9-hydroxyaflatoxin $B_1$ Adduct in the Adducted Duplex 5′-d(ACATC$^{AFB}$GATCT)-3′·5′-d(AGATCAATGT)-3′, Containing the Mismatched $C^5$·$A^{16}$ Pairing Interaction

| | |
|---|---|
| **Experimental Restraints** | |
| total NOE-derived distance restraints | 445 |
| internucleotide distance restraints | 305 |
| intranucleotide distance restraints | 110 |
| DNA−$AFB_1$ distance restraints | 30 |
| deoxyribose pseudorotation restraints | 15 |
| **Empirical Restraints** | |
| phosphodiester torsion angle restraints | 93 |
| H-bond restraints | 33 |
| **Structural Statistics** | |
| NMR *R*-factor ($R_1^x$) [a,b] | |
| ⟨$rMDR_{Ba}$⟩ | 0.089 ± 0.007 |
| root-mean-square deviations from ideal geometry[c] | |
| rmsd of NOE violations (Å) | 0.060 ± 0.001 |
| number of NOE violations > 0.2 Å in the entire duplex | 11 |
| improper angle (deg) | 0.33 ± 0.03 |
| pairwise rmsd (Å) over all atoms[c] | |
| ⟨$rMDr_{and}$⟩ vs ⟨rMDB⟩ | 1.15 ± 0.15 |

[a] The final PDB file obtained from AMBER was used for calculation. The mixing time was 180 ms. All values for $R_1^x$ are $\times 10^2$. [b] $R_1^x = \sum|(a_o)_i^{1/6} - (a_c)_i^{1/6}|/\sum|(a_o)_i^{1/6}|$, where $(a_o)$ and $(a_c)$ are the intensities of observed (nonzero) and calculated NOE cross-peaks. [c] ⟨$rMD_{rand}$⟩, average of 10 converged structures generated from rMD calculations starting from random coordinates; ⟨rMDB⟩, average of 10 converged structures starting from B-DNA coordinates, using X-PLOR.

[2] The definitions of the enantiotopic protons at C2 and C3 are based upon the Cahn, Ingold, and Prelog nomenclature. We defined H2α to be the *pro-R* proton at C2; H2$\beta$ is defined to be the *pro-S* proton at C2. H3α is defined to be the *pro-S* proton at C3, and H3$\beta$ is defined to be the *pro-R* proton at C3. H2α and H3α lie on the same face of the cyclopentenone ring, as do H6a and H9a; H2$\beta$ and H3$\beta$ lie on the other face of the cyclopentenone ring.

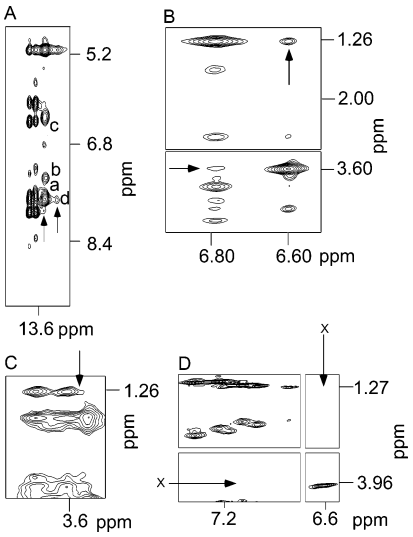


FIGURE 4: Tile plots showing NOEs associated with a minor conformation for base pairs $T^4$·$A^{17}$ and mismatched $C^5$·$A^{16}$. (A) Far downfield region of the $^1$H spectrum. Cross-peaks arising from the wobble $C^5$·$A^{16}$ base pair: a, overlap of three resonances, $T^{18}$ N3H → $A^3$ H2, $T^{18}$ N3H → $A^3$ $N^6H_a$, and $T^4$ N3H → $A^{17}$ H2; b, $T^4$ N3H → $A^{17}$ $N^6H_a$; c, overlap of two resonances, $T^{18}$ N3H → $A^3$ $N^6H_b$ and $T^4$ N3H → $A^{17}$ $N^6H_b$. Resonance d, arising from a minor conformation involving base pairs $T^4$·$A^{17}$ and mismatched $C^5$·$A^{16}$, assigned as overlap of two resonances, $T^4$ N3H → $A^{16}$ $N^6H_a$ and $T^4$ N3H → $A^{16}$ H2. The 800.13 MHz spectrum was collected at 150 ms mixing time, and 0 °C. (B) Aromatic region of the $^1$H spectrum. The arrows indicate NOEs between $AFB_1$ H6a → $T^4$ $CH_3$ ($\delta$ 6.6 ppm, $\delta$ 1.26 ppm), and between $AFB_1$ 4-$OCH_3$ → $T^4$ H6 ($\delta$ 3.6 ppm, $\delta$ 6.8 ppm). (C) Upfield region of the $^1$H spectrum. The arrow indicates a NOE between $AFB_1$ 4-$OCH_3$ → $T^4$ $CH_3$ ($\delta$ 3.6 ppm, $\delta$ 1.26 ppm). (D) Cross-peaks between $AFB_1$ H6a and $T^4$ $CH_3$, and between $AFB_1$ 4-$OCH_3$ and $T^4$ H6 are not observed in the spectrum of d(ACATC$^{AFB}$GATCT)·d(AGATCGATGT), having normal base pairing at base pair $C^5$·$G^{16}$ (*30*).

5′-intercalation of the $AFB_1$ moiety and the orientation of the 5′-neighbor $C^5$·$A^{16}$ mismatched base pair.

*E. Dihedral Torsion Angles.* The deoxyribose pseudorotation values were derived from analysis of $^1$H DQF−COSY spectra. These were found to be within the expected C2′-endo range, with the exception of the deoxyribose of mismatched nucleotide $C^5$. The calculated sugar puckering of the mismatched deoxycytosine was C3′-exo. It was not possible to measure heteronuclear $^{31}$P−$^1$H coupling constants necessary to restrain phosphodiester backbone torsion angles because the spectra were obtained at low temperature to minimize sample degradation.

*Structural Analysis*. The wobble pair at $C^5$·$A^{16}$ was modeled using two sets of rMD calculations. In the first, the mismatched $A^{16}$ was protonated at the N1 position. In the second, the mismatched $A^{16}$ was not protonated. Each set of calculations utilized 445 experimental distance restraints derived from nonexchangeable $^1$H NOEs. These consisted of 309 intranucleotide restraints and 136 internucleotide restraints, among which 42 were $AFB_1$−DNA restraints. The inter- and intranucleotide restraints were approximately evenly distributed along the length of the oligodeoxynucleotide, except for $T^{14}$ and $A^{15}$ (Figure 5). Fifteen deoxyribose pseudorotation restraints were derived from DQF-COSY data, and 33 hydrogen bonding restraints derived from observation of Watson Crick hydrogen bonding in the NMR spectra, were used. In addition to the experimentally derived restraints, 93 empirical backbone torsion angle restraints were used. The restraints used for these two sets of rMD calculations, along with the upper and lower bounds of distance restraints, are collected in Table S4 of the Supporting Information.

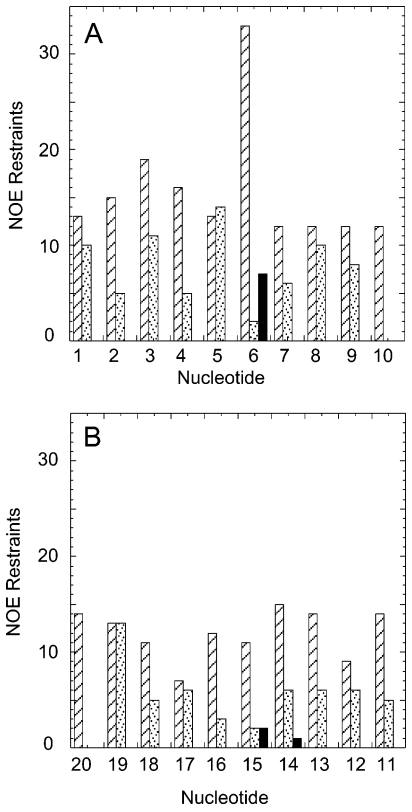


FIGURE 5: Distribution of NOE restraints used for rMD calculations of the protonated and nonprotonated wobble pairs at $C^5$·$A^{16}$. (A) Adducted strand. (B) Complementary strand. The bars with diagonal crosshatching represent intranucleotide NOEs, the stippled bars represent internucleotide NOEs, and the black bars indicate $AFB_1$−DNA NOEs.

The precision of both sets of rMD calculations as monitored by pairwise rmsd measurements (*67*) was excellent, particularly at and adjacent to the aflatoxin lesion and neighboring $C^5$·$A^{16}$ mismatch site (Figure 6). This site was well-defined by NOEs between the $AFB_1$ moiety and the DNA duplex. The degree of convergence was less at the terminal base pairs, consistent with the lower number of experimental restraints. For the calculations carried out on the unprotonated oligodeoxynucleotide, the maximum pairwise rmsd for the 20 structures calculated from the IniB starting structure was 0.55 Å, and 0.30 Å for 20 structures calculated from the randomized coordinates. The maximum pairwise rmsd for twenty structures calculated from protonated IniB was 0.35 Å.

*Complete Relaxation Matrix Calculations*. The two structures emergent from the rMD calculations on the protonated or nonprotonated wobble pairs were evaluated by complete relaxation matrix analysis using CORMA (*62*). This allowed theoretical NOE intensities to be compared with experimental NOE intensities. Overall, for the duplex oligodeoxynucleotides containing either the protonated or nonprotonated wobble structures, this approach yielded sixth root residuals of approximately 9.1%. The presence or absence of protonation at wobble pair $C^5$·$A^{16}$ had minimal effect on the overall sixth root residuals. This was consistent with the

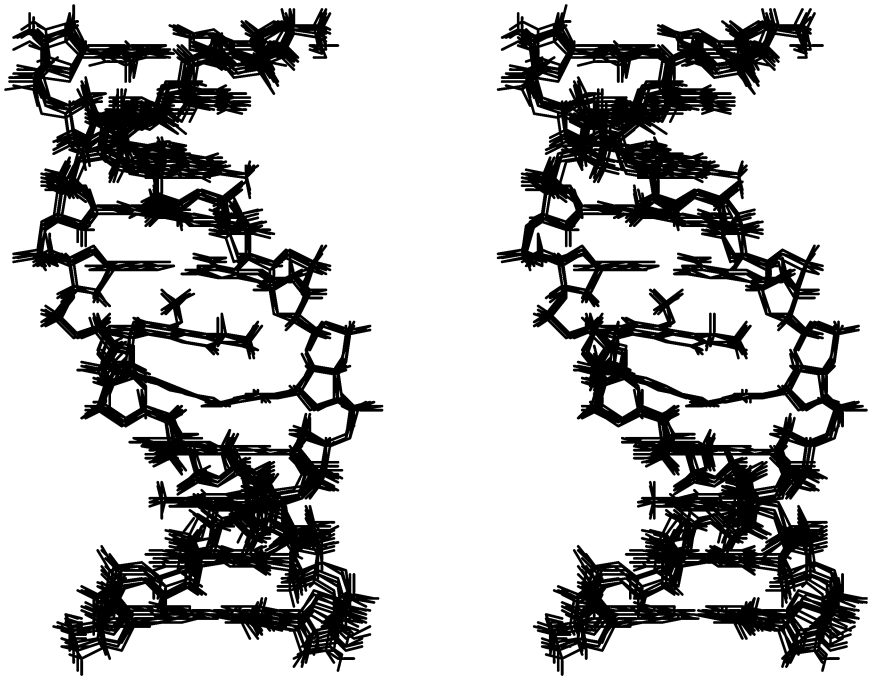

FIGURE 6: Stereo drawing of a superposition showing 20 structures emergent from rMD calculations which were initiated from a nonprotonated B-DNA starting conformation, using XPLOR. Excellent convergence was obtained at and adjacent to the $^{AFB}G^{6}$ lesion site and the $C^{5}\cdot A^{16}$ wobble pair.

expectation that protonation of adenine N1 in the wobble pair should not have a large impact upon the pattern or magnitude of NOEs at the lesion site. Significantly however, for either the protonated or nonprotonated wobble structures, base pairs $T^{4}\cdot A^{17}$ and $C^{5}\cdot A^{16}$ located 5′ to the $AFB_1$ damage site exhibited 15−20% sixth root residuals. Thus, these CORMA calculations suggested that neither the protonated nor the nonprotonated wobble pair at $C^{5}\cdot A^{16}$ accounted satisfactorily for all of the experimental NOEs at these two base pairs located 5′ to the $AFB_1$ damage site. This observation suggested the existence of a minor conformation, to be discussed below.

*Structure of the $C^{5}\cdot A^{16}$ Wobble Pair 5′ to the $AFB_1$ Adduct.* Both sets of rMD calculations yielded similar structures for the $AFB_1$-adducted oligodeoxynucleotide. The $AFB_1$ moiety intercalated above the 5′ face of the modified guanine, such that the $AFB_1-OCH_3$ and cyclopentenone ring protons faced into the minor groove, whereas the furofuran ring protons faced into the major groove (Figure 7). The presence of the $AFB_1$ moiety resulted in a rise of 7.8 Å between $^{AFB}G^{6}\cdot C^{15}$ and mismatched $C^{5}\cdot A^{16}$, as compared to the value of 3.4 Å observed for B-DNA. These two base pairs buckled in opposite directions away from the intercalated $AFB_1$ moiety. Helicoidal buckle measurements, of 22° and −12°, were calculated for $C^{5}\cdot A^{16}$ and $^{AFB}G^{6}\cdot C^{15}$, respectively, similar to previous studies (*31*, *34*) and to intercalation structures determined crystallographically (*68*, *69*). The mispairing of adenine opposite $C^{5}$ resulted in unwinding of the helix as compared to $C^{5}\cdot G^{16}$ in the correctly paired d(ACATC$\underline{C}^{AFB}$GATCT)·d(AGATCGATGT) $AFB_1$-modified duplex (*31*) (Figure 8).

*Conformation of the $C^{5}\cdot A^{16}$ Wobble Pair*. Stacking interactions for both the protonated and nonprotonated wobble pairs were compared with the stacking of the correct $C^{5}\cdot G^{16}$ base pair 5′ to the $AFB_1$ lesion in d(ACATC$^{AFB}$GATCT)·d(AGATCGATGT) (*30*, *31*) (Figure 8). Formation of the

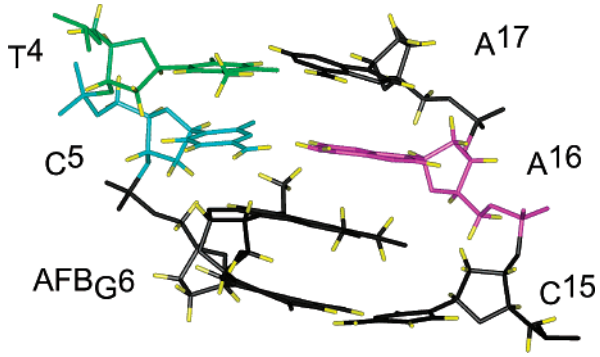


FIGURE 7: View of base pairs $T^{4}\cdot A^{17}$, $C^{5}\cdot A^{16}$, and $^{AFB}G^{6}\cdot C^{15}$ from the major groove. The $AFB_1$ moiety is intercalated above the 5′ face of the guanine nucleobase in $^{AFB}G^{6}$. The $AFB_1$ H5 and 4-$OCH_3$ protons face into the minor groove. The $AFB_1$ H6a and H9a protons face in the major groove in the 5′ direction. Unwinding of the duplex and an increased rise is observed at the intercalation site. The wobble base pair $C^{5}\cdot A^{16}$ stacks above the $AFB_1$ moiety and is contained within the helix. Protons are indicated in yellow. Nucleotide $T^{4}$ is green, nucleotide $C^{5}$ is blue, and nucleotide $A^{16}$ is purple.

protonated $C^{5}\cdot A^{16}$ mismatch shifted $C^{5}$ toward the major groove and shifted $A^{16}$ toward the minor groove, as a result of the hydrogen bond between $A^{16}$ N1 and $C^{5}$ N3H (Scheme 2). This resulted in the stacking of $C^{5}$ directly below $T^{4}$ and may account for the upfield shift of $T^{4}$ H6 and downfield shifts of $C^{5}$ H5 and H6 observed in Figure 1. It may also account for the weaker NOE observed from $C^{5}$ H1′ → $A^{16}$ H8. The mismatched $A^{16}$ stacked well with the $AFB_1$ moiety, which perhaps accounted for the increase in $T_m$ as compared to the same $C^{5}\cdot A^{16}$ mismatch in the absence of the damaged nucleotide $^{AFB}G^{6}$.

*A Minor Conformation Involving Base Pairs $T^{4}\cdot A^{17}$ and $C^{5}\cdot A^{16}$*. The CORMA calculations discussed above suggested the presence of a minor conformation. A small NOE was observed between $T^{4}$ $CH_3$ and $AFB_1$ H6a, as was an NOE

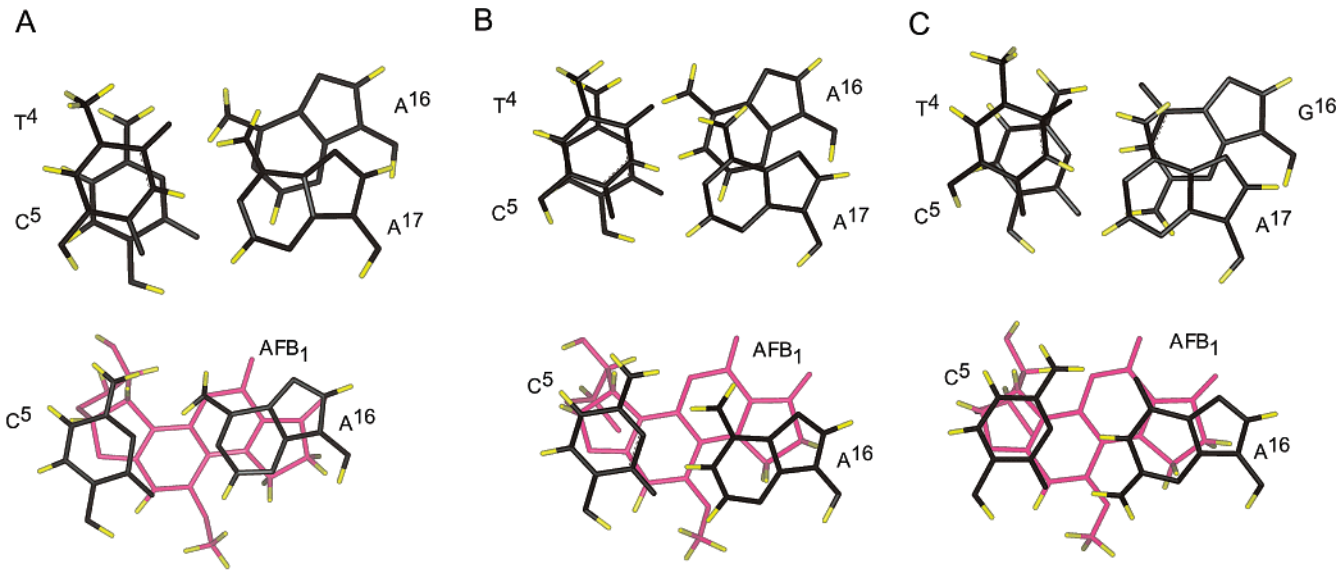


FIGURE 8: Stacking interactions of the protonated and nonprotonated $C^5$·$A^{16}$ wobble pair as predicted by rMD calculations. (A) The nonprotonated wobble pair. At the top is the stacking of $T^4$·$A^{17}$ above $C^5$·$A^{16}$. Below is the stacking of $C^5$·$A^{16}$ above the $AFB_1$ moiety of $^{AFB}G^6$. (B) The protonated wobble pair. At the top is the stacking of $T^4$·$A^{17}$ above $C^5$·$A^{16}$. Below is the stacking of $C^5$·$A^{16}$ above the $AFB_1$ moiety of $^{AFB}G^6$. (C) Stacking interactions of the normal $C^5$·$G^{16}$ base pair as predicted by rMD calculations (*30*, *31*). At the top is the stacking of $T^4$·$A^{17}$ above $C^5$·$G^{16}$. Below is the stacking of $C^5$·$G^{16}$ above the $AFB_1$ moiety of $^{AFB}G^6$. Protons are indicated in yellow. The $AFB_1$ moiety is indicated in purple. In the protonated wobble pair, the rMD calculations predict stacking of $T^4$ above $C^5$ due to the shift of $C^5$ toward the minor groove. This may account for the unusual upfield shift of the $T^4$ H6 resonance. Also, note the favorable stacking interactions of wobble pair $C^5$·$A^{16}$ above the $AFB_1$ moiety.

between $T^4$ H6 and $AFB_1$ 4-$OCH_3$. $T^4$ $CH_3$ and H6 also showed a small NOE to $AFB_1$ H9a. In addition, a small NOE was observed between $T^4$ $CH_3$ and $AFB_1$ $OCH_3$. That these were observed over a range of mixing times from 130 to 250 ms suggested they did not result from spin diffusion. These were unexpected since $T^4$ was the second nucleotide in the 5′ direction from $^{AFB}G^6$; hence, it would not have been expected to show NOEs to $^{AFB}G^6$. Moreover, similar NOEs between $T^4$ and $AFB_1$ protons were not observed in spectra of d(ACATC$^{AFB}$GATCT)·d(AGATCGATGT), having normal base pairing at base pair $C^5$·$G^{16}$ (*30*, *31*). The NOEs between $T^4$ and the $AFB_1$ protons of $^{AFB}G^6$ suggested an unusually close proximity between nucleotides $T^4$ and $^{AFB}G^6$ in the minor conformation. A broad resonance was observed in the imino region of the spectrum at $\delta$ 13.4 ppm (Figure 2). Its integral did not correspond with those of the assigned imino proton resonances. This resonance exhibited a weak NOE to a resonance at $\delta$ 7.65 ppm and showed an exchange peak with the water resonance. It also showed an exchange peak with the overlapped resonances of $T^4$ H3 and $T^{18}$ H3 observed at $\delta$ 13.5 ppm. The possibility that this resonance arose from the terminal thymine imino resonances was discarded by the observation of $T^{10}$ N3H and $T^{20}$ N3H as weak signals at approximately 13 ppm. It was also attributed to a minor conformation involving $T^4$ N3H. The small presence of the minor conformation and the small number of resonances attributed to it precluded its structural refinement.

## DISCUSSION

The nontargeted C → T mutations induced by the cationic guanine N7 8,9-dihydro-8-(N7-guanyl)-9-hydroxy aflatoxin $B_1$ adduct at nucleotide $C^5$, 5′ to a modified $^{AFB}G^6$·$C^{15}$ pair (*28*), correlated with structural studies which have consistently shown the cationic $AFB_1$ lesion to be intercalated above the 5′-face of the modified deoxyguanosine nucleotide (*29*, *32*−*34*). The existence of these nontargeted mutations is of interest, in part because it indicates that site-specific DNA damage can induce specific mutations at adjacent nondamaged base pairs. The modified $^{AFB}G^6$·$C^{15}$ pair having a 5′-neighbor $C^5$·$A^{16}$ mismatch examined in the present study models the situation that exists in duplex DNA after incorrect incorporation of dATP opposite $C^5$, 5′ to the cationic guanine N7 $AFB_1$ lesion located at $^{AFB}G^6$.

*Wobble Base Pairing at the Mismatch Site.* The mismatched $C^5$·$A^{16}$ base pair adjacent to the modified $^{AFB}G^6$·$C^{15}$ pair existed in the wobble conformation. In this conformation, the imino nitrogen $C^5$ N3 formed a hydrogen bond with the $A^{16}$ exocyclic amine. The result was a shift of the mispaired $A^{16}$ toward the minor groove, accompanied by a shift of the mispaired $C^5$ toward the major groove (Figures 7 and 8). The insertion of $A^{16}$ into the duplex was established by NOEs between the $A^{16}$ amino protons and $T^4$ $CH_3$ at the 5′-neighbor base pair $T^4$·$A^{17}$. The amino protons of $A^{16}$ also showed the expected NOE to the $NH_2$ group of mismatched $C^5$. That only one resonance was observed for both the amino protons of the mismatched $C^5$ confirmed that the $A^{16}$ amino protons and not the $C^5$ amino groups participated in the hydrogen bonding (*36*). The rMD calculations predicted that $C^5$ stacked with $T^4$. The weaker-than-expected NOEs between $AFB_1$ H6a and $C^5$ H5 and H6 and between $AFB_1$ H9a and $C^5$ H5, and the lack of an NOE between $AFB_1$ H9a and $C^5$ H6, were consistent with the shift of $C^5$ toward the major groove in the wobble pair. The weak NOEs observed between the $AFB_1$ cyclopentenone protons and mismatched $A^{16}$ were consistent with the notion that $A^{16}$ shifted toward the minor groove in the wobble pair, resulting in greater distance between the minor groove $A^{16}$ H2 proton and $AFB_1$ H2α, H3α protons.

*Protonation State of Adenine in the Wobble Pair*. The wobble pair $C^5 \cdot A^{16}$ existed as an equilibrium blend of the protonated and nonprotonated forms. It was not possible to establish the p$K_a$ of the $A^{16}$ N1 at the $C^5 \cdot A^{16}$ wobble pair because the cationic $AFB_1$ adduct $^{AFB}G^6$ underwent depurination as pH was lowered and underwent conversion to the corresponding formamidopyrmidine (FAPY) derivative as pH was raised. It was not possible to identify a resonance from the protonated $A^{16}$ imine, presumably due to rapid exchange with solvent. The broadening of the $C^5$ H5 and H6 resonances and of the $A^{16}$ H8 resonance (Figure 1) was attributed to proton exchange at $A^{16}$ N1. This suggested a similar p$K_a$ for the wobble mismatch in the presence of $AFB_1$. Presumably, formation of a second hydrogen bond between $C^5$ $O^6$ and the protonated $A^{16}$ imine stabilized the wobble pair. It may be further stabilized by favorable stacking interactions with the cationic $AFB_1$ adduct located at $^{AFB}G^6 \cdot C^{15}$ (Figure 8). The presence of a significant population of the protonated $C^5 \cdot A^{16}$ wobble pair was consistent with the 8 °C increase in the $T_m$ value of the mispaired oligodeoxynucleotide. Parallel studies of the unmodified d(ACATCGATCT)(AGATCAATGT) duplex, which lacked the $AFB_1$ adduct, were instructive. In those studies, at neutral pH, the $A^{16}$ H8 resonance was broad, presumably due to proton exchange at adenine N1. At pH 4.8, the $A^{16}$ H8 resonance sharpened and shifted 0.3 ppm downfield. This was consistent with previous studies on C·A mismatches that suggested p$K_a$ for adenine N1 in a wobble C·A pair was near pH 7 (*38*, *39*, *70*).

*Aflatoxin Adduct Structure*. The orientation of the aflatoxin $B_1$ moiety in the presence of the 5′-neighboring wobble pair was reminiscent of previously refined structures of site-specific aflatoxin $B_1$ adducts (*31*−*34*). The $^{AFB}G^6$ protons had similar chemical shifts and showed NOEs to the 5′-flanking $C^5 \cdot A^{16}$ wobble pair. This structural motif appears to be a characteristic of the cationic guanine N7 $AFB_1$ adduct, which is conserved irrespective of the nature of the 5′ flanking base pair. However, the shift of $C^5$ toward the major groove and of $A^{16}$ toward the minor groove in the protonated $C^5 \cdot A^{16}$ wobble pair altered the distribution and intensities of NOEs, particularly between $AFB_1$ H6a and H9a, facing in the 5′ direction, and protons of the wobble pair.

*Structural Hypothesis for the Minor Conformation*. The small number and low intensity of the unexpected NOEs assigned to the minor conformation precluded the extraction of detailed structural information from the spectra. The observation that they were between $T^4$ $CH_3$ and $T^4$ H6 and the $AFB_1$ protons (Figure 4) suggested that they arose from a conformation in which $T^4$ was closer to the $AFB_1$ moiety than expected. Model building suggested a possible explanation. If $C^5$ were to be transiently dislocated from the duplex, this would allow pairing of $T^4$ with $A^{16}$ (the mismatched dA), instead of $A^{17}$ (its complement). This hypothesis was examined using PEM calculations restrained by the $T^4 \cdot A^{16}$ pairing, and leaving $C^5$ and $A^{17}$ unpaired.

The model structure (Figure 9) was consistent with spectroscopic observations. Proton exchange between protonated and nonprotonated wobble pairs at position $C^5 \cdot A^{16}$ did not easily account for spectral broadening of the $T^4 \cdot A^{17}$ resonances (Figure 1), since the structures of the protonated and nonprotonated wobble pairs are similar (Figure 8). On the other hand, equilibration of $T^4$ between a major $T^4 \cdot A^{17}$ and a minor $T^4 \cdot A^{16}$ conformation might account for the

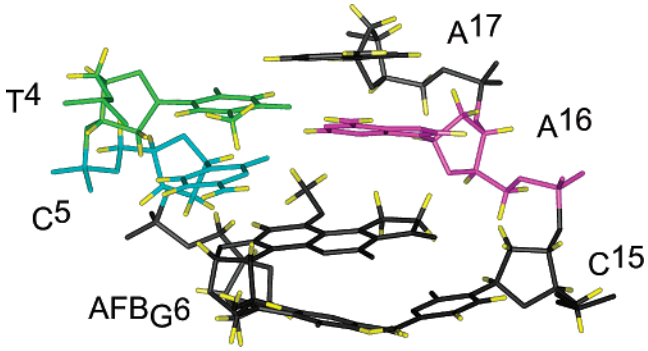


FIGURE 9: A possible structure for the minor conformation involving base pairs $T^4 \cdot A^{17}$ and mismatched $C^5 \cdot A^{16}$ derived from molecular modeling studies. Transient dislocation of $C^5$ allows formation of a $T^4 \cdot A^{16}$ pair above $^{AFB}G^6$, leaving $C^5$ and $A^{17}$ unpaired. This brings $T^4$ into proximity of the $AFB_1$ moiety and accounts for the unexpected NOEs between $T^4$ H6 and $T^4$ $CH_3$ and the $AFB_1$ moiety.

observed broadening of spectral lines at base pair $T^4 \cdot A^{17}$. In addition, Figure 9 suggested transient base pairing of $T^4$ with $A^{16}$ could place $T^4$ $CH_3$ proximate to the $AFB_1$ moiety at $^{AFB}G^6$, potentially explaining the unusual NOEs between $T^4$ and $^{AFB}G^6$ (Figure 4). Also, the model structure suggested that cross-peak "d" in Figure 4 resulted from dipolar coupling between $T^4$ N3H and the hydrogen bonded amino proton of $A^{16}$. It might also include a contribution from dipolar coupling between $T^4$ N3H and $A^{16}$ H2, although the H2 resonance arising from the minor conformation was not unequivocally identified.

*Implications for Nontargeted Mutagenesis 5′ to the Cationic Guanine N7 Adduct of AFB₁*. In *E. coli*, error-prone bypass of the cationic $AFB_1$ lesion is dependent upon the presence of the UmuDC or MucAB damage-specific polymerases (*28*). The formation of the $C^5 \cdot A^{16}$ wobble pair 5′ to the $AFB_1$ moiety at $^{AFB}G^6$ during error-prone replication, if not subsequently repaired, would yield the observed nontargeted C → T transitions induced by the cationic guanine N7 $AFB_1$ lesion (*28*). The present observation that the $C^5 \cdot A^{16}$ wobble pair is stable and is accommodated by the DNA duplex without major distortion suggests that it might allow for 3′-primer extension at $A^{16}$. The extent to which the wobble $C^5 \cdot A^{16}$ pair studied here in duplex DNA exists in the presence of a damage-specific replication apparatus and facilitates primer extension, remains to be determined. However, damage-specific Y-family DNA polymerases probably facilitate error-prone replication bypass, in part, by relaxing the geometric constraints for correct nucleotide incorporation at the active site (*71*).

DNA replication errors involving transient strand slippage were postulated by Streisinger to generate frameshift mutations (*72*, *73*). Kunkel and Alexander (*40*, *41*) suggested transient strand slippage, followed by realignment prior to subsequent extension of the replication complex, might also cause point mutations. They termed this "dislocation mutagenesis". Dislocation mutagenesis might explain nontargeted C → T mutations 5′ to the $^{AFB}G$ lesion in *E. coli (28)*. In this scenario (Scheme 3), after correct incorporation of dCTP opposite $^{AFB}G$, the 5′-neighbor cytosine would undergo transient dislocation, enabling the next-nearest 5′-neighbor thymine to template for an incoming dATP. Relaxation of the transient dislocation structure would result in formation of the C·A mismatch 5′ to the $^{AFB}G$ lesion.

Scheme 3: A Possible Mechanism for Nontargeted C → T Transitions Induced by the Cationic Guanine N7 $AFB_1$ Adduct[a]

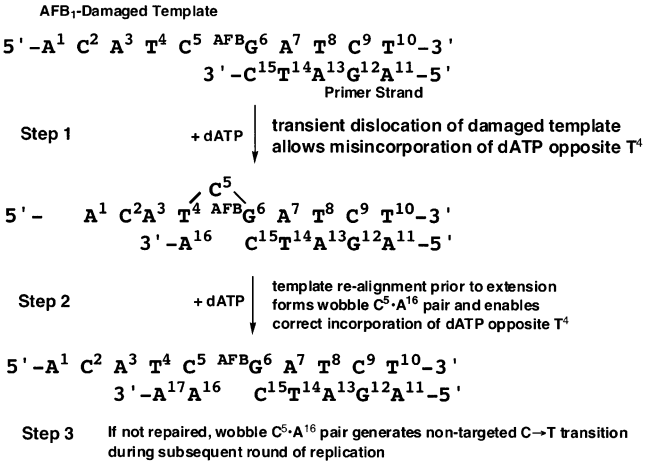


[a] Transient strand dislocation allows $T^4$ to template for an incoming dATP. Relaxation of the dislocation complex to form the $C^4$•$A^{15}$ wobble pair prior to extension then allows $T^4$ to template for an incoming dATP. If the wobble pair is not repaired, it leads to a nontargeted C → T transition in a subsequent round of replication.

The proposed structure of a minor conformation in equilibrium with the wobble pair $C^5$•$A^{16}$ adjacent to the cationic guanine N7 $AFB_1$ lesion (Figure 9) suggests that the cationic guanine N7 adduct of $AFB_1$ might facilitate transient strand slippage in duplex DNA. The extent to which a similar dislocation of $C^5$ might occur at the moment of replication, enabling $T^4$ to template for an incoming dATP and forming a transient $T^4$•$A^{16}$ pair adjacent to $^{AFB}G^6$, is not known. It is of interest that crystallographic studies of the Y-family *dinB* homologue polymerase from *Sulfolobus solfataricus* revealed a relaxed active site geometry characterized by two template bases entering the active site (*74*). A transient dislocation intermediate involving the cationic guanine N7 adduct of $AFB_1$ might be accommodated by the UmuDC or MucAB damage-specific polymerases in *E. coli*.

Upon the basis of their observation of $AFB_1$-induced nontargeted 5′ C → T mutations in *E. coli*, Bailey et al. (*28*) suggested the possibility that mutation data from forward assays utilizing metabolically activated $AFB_1$ might have been mistakenly scored. Specifically, nontargeted $AFB_1$-induced mutations located 5′ to adducted deoxyguanosines might have been misinterpreted as resulting from adjacent $AFB_1$-modified deoxyguanosines in either the template or the primer strand. If transient dislocation of the damaged template accounts for some of these nontargeted $AFB_1$ mutations, the spectrum of such mutations should depend on the sequence context 5′ to the $^{AFB}G$ damage site in DNA.

*Summary*. The present results show that the mismatched $C^5$•$A^{16}$ base pair located 5′ to an $^{AFB}G$ damage site exists predominantly in the wobble conformation, which at neutral pH exists as a mixture of the protonated and nonprotonated species. The wobble pair is accommodated by the adducted DNA duplex with minor additional perturbation. It might provide an effective template for strand extension. If not repaired, it would result in the observed nontargeted C → T mutations observed by Bailey et al. (*28*), which occurred 5′ to an $^{AFB}G$ damage site. The $C^5$•$A^{16}$ wobble pair exists in equilibrium with a minor conformation. While it has not been possible to obtain a refined structure of the minor conformation, the available data suggest that it arises from a transient dislocation structure, in which $T^4$ is paired not with $A^{17}$, but rather with the mismatched $A^{16}$. The formation of such a structure during error-prone replication might provide a mechanism for the nontargeted C → T mutations located 5′ to a $^{AFB}G$ damage site (*28*).

## SUPPORTING INFORMATION AVAILABLE

Figures showing atomic names and types used for AMBER calculations, and the partial charges, as well as the expanded sequential NOE connectivities. Tables showing $^1H$ NMR chemical shift assignments and the experimental distances and classes of restraints. This material is available free of charge via the Internet at http://pubs.acs.org.

## REFERENCES

1. Busby Jr., W. F., and Wogan, G. N. (1984) in *Chemical Carcinogens* (Searle, C. E., Ed.) pp 945−1136, American Chemical Society, Washington, DC.
2. McCann, J., Spingarn, N. E., Koburi, J., and Ames, B. N. (1975) *Proc. Natl. Acad. Sci. U.S.A. 72*, 979−983.
3. Foster, P. L., Eisenstadt, E., and Miller, J. H. (1983) *Proc. Natl. Acad. Sci. U.S.A. 80*, 2695−2698.
4. Foster, P. L., Groopman, J. D., and Eisenstadt, E. (1988) *J. Bacteriol. 170*, 3415−3420.
5. Bailey, G. S., Loveland, P. M., Pereira, C., Pierce, D., Hendricks, J. D., and Groopman, J. D. (1994) *Mutat. Res. 313*, 25−38.
6. Bailey, G. S., Williams, D. E., Wilcox, J. S., Loveland, P. M., Coulombe, R. A., and Hendricks, J. D. (1988) *Carcinogenesis 9*, 1919−1926.
7. McMahon, G., Davis, E. F., Huber, L. J., Kim, Y., and Wogan, G. N. (1990) *Proc. Natl. Acad. Sci. U.S.A. 87*, 1104−1108.
8. Soman, N. R., and Wogan, G. N. (1993) *Proc. Natl. Acad. Sci. U.S.A. 90*, 2045−2049.
9. Bressac, B., Kew, M., Wands, J., and Ozturk, M. (1991) *Nature 350*, 429−431.
10. Hsu, I. C., Metcalf, R. A., Sun, T., Welsh, J. A., Wang, N. J., and Harris, C. C. (1991) *Nature 350*, 427−428.
11. Greenblatt, M. S., Bennett, W. P., Hollstein, M., and Harris, C. C. (1994) *Cancer Res. 54*, 4855−4878.
12. Shen, H. M., and Ong, C. N. (1996) *Mutat. Res. 366*, 23−44.
13. Soini, Y., Chia, S. C., Bennett, W. P., Groopman, J. D., Wang, J. S., DeBenedetti, V. M., Cawley, H., Welsh, J. A., Hansen, C., Bergasa, N. V., Jones, E. A., DiBisceglie, A. M., Trivers, G. E., Sandoval, C. A., Calderon, I. E., Munoz Espinosa, L. E., and Harris, C. C. (1996) *Carcinogenesis 17*, 1007−1012.
14. Lunn, R. M., Zhang, Y. J., Wang, L. Y., Chen, C. J., Lee, P. H., Lee, C. S., Tsai, W. Y., and Santella, R. M. (1997) *Cancer Res. 57*, 3471−3477.
15. Mace, K., Aguilar, F., Wang, J. S., Vautravers, P., Gomez-Lechon, M., Gonzalez, F. J., Groopman, J., Harris, C. C., and Pfeifer, A. M. (1997) *Carcinogenesis 18*, 1291−1297.
16. Santella, R. M., Zhang, Y. J., Chen, C. J., Hsieh, L. L., Lee, C. S., Haghighi, B., Yang, G. Y., Wang, L. W., and Feitelson, M. (1993) *Environ. Health Perspect. 99*, 199−202.
17. Chen, C. J., Yu, M. W., Liaw, Y. F., Wang, L. W., Chiamprasert, S., Matin, F., Hirvonen, A., Bell, D. A., and Santella, R. M. (1996) *Am. J. Hum. Genet. 59*, 128−134.
18. Yu, M. W., Lien, J. P., Chiu, Y. H., Santella, R. M., Liaw, Y. F., and Chen, C. J. (1997) *J. Hepatol. 27*, 320−330.
19. Ueng, Y. F., Shimada, T., Yamazaki, H., and Guengerich, F. P. (1995) *Chem. Res. Toxicol. 8*, 218−225.
20. Baertschi, S. W., Raney, K. D., Stone, M. P., and Harris, T. M. (1988) *J. Am. Chem. Soc. 110*, 7929−7931.
21. Johnson, W. W., Harris, T. M., and Guengerich, F. P. (1996) *J. Am. Chem. Soc. 118*, 8213−8220.
22. Essigmann, J. M., Croy, R. G., Nadzan, A. M., Busby Jr., W. F., Reinhold, V. N., Buchi, G., and Wogan, G. N. (1977) *Proc. Natl. Acad. Sci. U.S.A. 74*, 1870−1874.
23. Gopalakrishnan, S., Stone, M. P., and Harris, T. M. (1989) *J. Am. Chem. Soc. 111*, 7232−7239.

24. Iyer, R. S., Coles, B. F., Raney, K. D., Thier, R., Guengerich, F. P., and Harris, T. M. (1994) *J. Am. Chem. Soc. 116*, 1603−1609.
25. Green, C. L., Loechler, E. L., Fowler, K. W., and Essigmann, J. M. (1984) *Proc. Natl. Acad. Sci. U.S.A. 81*, 13−17.
26. Loechler, E. L., Green, C. L., and Essigmann, J. M. (1984) *Proc. Natl. Acad. Sci. U.S.A. 81*, 6271−6275.
27. Basu, A. K., and Essigmann, J. M. (1988) *Chem. Res. Toxicol. 1*, 1−18.
28. Bailey, E. A., Iyer, R. S., Stone, M. P., Harris, T. M., and Essigmann, J. M. (1996) *Proc. Natl. Acad. Sci. U.S.A. 93*, 1535−1539.
29. Gopalakrishnan, S., Harris, T. M., and Stone, M. P. (1990) *Biochemistry 29*, 10438−10448.
30. Jenkins, M. D. (2000) Thesis (M.S. in Chemistry), Vanderbilt University, Nashville, TN.
31. Giri, I., Jenkins, M. D., Schnetz-Boutaud, N. C., and Stone, M. P. (2002) *Chem. Res. Toxicol. 15*, 638−647.
32. Jones, W. R., Johnston, D. S., and Stone, M. P. (1998) *Chem. Res. Toxicol. 11*, 873−881.
33. Giri, I., Johnston, D. S., and Stone, M. P. (2002) *Biochemistry 41*, 5462−5472.
34. Johnston, D. S., and Stone, M. P. (1995) *Biochemistry 34*, 14037−14050.
35. Gopalakrishnan, S., Liu, X., and Patel, D. J. (1992) *Biochemistry 31*, 10790−10801.
36. Patel, D. J., Kozlowski, S. A., Ikuta, S., and Itakura, K. (1984) *Biochemistry 23*, 3218−3226.
37. Gao, X., and Patel, D. J. (1987) *J. Biol. Chem. 262*, 16973−16984.
38. Sarma, M. H., Gupta, G., Sarma, R. H., Bald, R., Engelke, U., Oei, S. L., and Gessner, R. (1987) *Biochemistry 26*, 7707−7715.
39. Hunter, W. N., Brown, T., Anand, N. N., and Kennard, O. (1986) *Nature 320*, 552−555.
40. Kunkel, T. A., and Alexander, P. S. (1986) *J. Biol. Chem. 261*, 160−166.
41. Kunkel, T. A. (1990) *Biochemistry 29*, 8003−8011.
42. Murray, R. W., and Jeyaraman, R. (1985) *J. Org. Chem. 50*, 2847−2853.
43. Piotto, M., Saudek, V., and Sklenar, V. (1992) *J. Biomol. NMR 6*, 661−665.
44. Rinkel, L. J., and Altona, C. (1987) *J. Biomol. Struct. Dyn. 4*, 621−649.
45. Borgias, B. A., and James, T. L. (1990) *J. Magn. Reson. 87*, 475−487.
46. Liu, H., Spielmann, H. P., Ulyanov, N. B., Wemmer, D. E., and James, T. L. (1995) *J. Biomol. NMR 6*, 390−402.
47. Kouchakdjian, M., Marinelli, E., Gao, X., Johnson, F., Grollman, A., and Patel, D. (1989) *Biochemistry 28*, 5647−5657.
48. Arnott, S., and Hukins, D. W. L. (1972) *Biochem. Biophys. Res. Comm. 47*, 1504−1509.
49. Frisch, M. J., Trucks, G. W., et al. (1998) *GAUSSIAN 98*, Gaussian, Inc., Pittsburgh, PA.
50. Petersson, G. A., Bennett, A., Tensfeldt, T. G., Al-Laham, M. A., Shirley, W. A., and Mantzaris, J. (1988) *J. Chem. Phys. 89*, 2193−2218.
51. Petersson, G. A., and Al-Laham, M. A. (1991) *J. Chem. Phys. 94*, 6081−6090.
52. Bayly, C. I., Cieplak, P., Cornell, W. D., and Kollman, P. A. (1993) *J. Phys. Chem. 40*, 10269−10280.
53. Brunger, A. T. (1992) *X-PLOR. Version 3.1., A System for X-ray Crystallography and NMR*, Yale University Press, New Haven, CT.
54. Nilsson, L., and Karplus, M. (1986) *J. Comput. Chem. 7*, 591−616.
55. Clore, G. M., Gronenborn, A. M., Carlson, G., and Meyer, E. F. (1986) *J. Mol. Biol. 190*, 259−267.
56. Ryckaert, J.-P., Ciccotti, G., and Berendsen, H. J. C. (1977) *J. Comput. Phys. 23*, 327−341.
57. Jorgensen, W. L., Chandrasekhar, J., Madura, J. D., Impey, R. W., and Klein, M. L. (1983) *J. Chem. Phys. 79*, 926−935.
58. Case, D. A., Pearlman, C. A., et al. (1999) *AMBER 6.0*, University of California, San Francisco.
59. Cornell, W. D., Cieplak, P., Bayly, C. I., Gould, I. R., Merz, K. M., Ferguson, D. M., Spellmeyer, D. C., Fox, T., Caldwell, J. W., and Kollman, P. A. (1995) *J. Am. Chem. Soc. 117*, 5179−5197.
60. Darden, T., York, D., and Pedersen, L. (1993) *J. Chem. Phys. 12*, 10089−10092.
61. Essmann, U., Perera, L., Berkowitz, M. L., Darden, T., Lee, H., and Pedersen, L. G. (1995) *J. Chem. Phys. 19*, 8577−8593.
62. Keepers, J. W., and James, T. L. (1984) *J. Magn. Reson. 57*, 404−426.
63. Liu, Y., Zhao, D., Altman, R., and Jardetzky, O. (1992) *J. Biomol. NMR 2*, 373−388.
64. Thomas, P. D., Basus, V. J., and James, T. L. (1991) *Proc. Natl. Acad. Sci. U.S.A. 88*, 1237−1241.
65. Lu, X. J., Shakked, Z., and Olson, W. K. (2000) *J. Mol. Biol. 300*, 819−840.
66. Reid, B. R. (1987) *Q. Rev. Biophys. 20*, 2−28.
67. Allain, F. H., and Varani, G. (1997) *J. Mol. Biol. 267*, 338−351.
68. Egli, M., Williams, L. D., Frederick, C. A., and Rich, A. (1991) *Biochemistry 30*, 1364−1372.
69. Frederick, C. A., F., Williams, L. D., Ughetto, G., van der Marel, G. A., van Boom, J. H., Rich, A., and Wang, A. H.-J. (1990) *Biochemistry 29*, 2538−2549.
70. Kalnik, M. W., Chang, C. N., Grollman, A. P., and Patel, D. J. (1988) *Biochemistry 27*, 924−931.
71. Goodman, M. F. (2002) *Annu. Rev. Biochem. 71, 17−50.*
72. Streisinger, G., Okada, Y., Enrich, J., Newton, J., Tsugita, A., Terzaghi, E., and Inouye, M. (1966) *Cold Spring Harbor Symp. Quantum Biol. 31*, 77−84.
73. Streisinger, G., and Owen, J. E. (1985) *Genetics 109*, 633−659.
74. Ling, H., Boudsocq, F., Woodgate, R., and Yang, W. (2001) *Cell 107*, 91−102.


BI020688N